

# Preparation and Characterization of $\text{Ag}_2\text{E}$ (E = Se, Te) Using the Sonochemically Assisted Polyol Method

R. Harpness,<sup>†</sup> O. Palchik,<sup>†</sup> A. Gedanken,<sup>\*,†</sup> V. Palchik,<sup>‡</sup> S. Amiel,<sup>‡</sup> M. A. Slifkin,<sup>‡</sup> and A. M. Weiss<sup>‡</sup>

Department of Chemistry, Bar-Ilan University, Ramat-Gan, 52900, Israel,  
and Department of Electronics, Jerusalem College of Technology, Jerusalem, 91160, Israel

Received August 27, 2001. Revised Manuscript Received December 4, 2001

Nanocrystals of  $\text{Ag}_2\text{E}$  (E = Se, Te) were prepared using the polyol reduction method under sonochemical irradiation. Particles were characterized using TEM, HRTEM, SEM, and XRD. The optical properties of the products were studied using photoacoustic spectroscopy (PAS). The differences between the as-prepared samples and single crystals and method of the nanoparticle formation are discussed.

## Introduction

Over the past few years there has been tremendous growth in the number of publications concerned with giant magnetoresistive (MR) compounds.<sup>1,2</sup> C. N. Rao considered GMR materials to be one of the four most important categories of materials at the end of the last century.<sup>3</sup> Devices based on GMR materials function at room temperatures and low magnetic fields. Many GMR compounds and engineered structures have been found. Examples of these compounds include magnetic multilayers,<sup>4</sup> manganite perovskites,<sup>5</sup> and a few others.<sup>6</sup> Recently, a new group of GMR materials was found among the non-oxide compounds. Classical non-oxide narrow gap semiconductors such as PbTe have large low field magnetoresistance at room temperature, but their characteristic resistivity is so large that the intrinsic device noise is limiting.<sup>1</sup> This problem motivated research to find new narrow gap GMR compounds with low resistivity ( $<10^4 \mu\Omega\text{-cm}$ ). Such materials were recently found in transition metal Zintl compounds,<sup>7</sup> chromium,<sup>8</sup> and iron sulfides.<sup>9</sup> These new compounds are not three-dimensional ferromagnets and do not show metallic behavior. This caused a revolution in the classical theories of MR, which require mixed valences and the operation of a double-exchange mechanism for a compound to be magnetoresistant.<sup>9</sup>

In this article, we present studies of a much less explored class of magnetoresistive compounds, the silver chalcogenides,  $\text{Ag}_2\text{Se}$  and  $\text{Ag}_2\text{Te}$ . A large, positive MR effect for these nonmagnetic compounds was recently discovered.<sup>1</sup> Both compounds are known as very good ionic conductors at room temperature<sup>10</sup> because of their low activation energy for diffusion and conduction. Both compounds are narrow-gap n-type semiconductors,<sup>11,12</sup> and in the exact stoichiometric ratio they do not show appreciable magnetoresistance.<sup>13</sup> However, a slight deviation from the exact stoichiometry results in a marked increase in their MR effect. It was shown by Rosenbaum and co-workers that, at room temperature, when subjected to a magnetic field of 55 kOe, the resistance of the nonstoichiometric phases of both silver chalcogenides increase by up to 200% relative to field-free conditions.<sup>1</sup> This measured resistance is comparable with that of GMR materials. The relatively low resistance and ease of the MR response at low fields make these compounds excellent candidates for applications requiring MR devices. Previous studies regarding these compounds were concerned with single crystals or thin films. Silver selenide was prepared in the past by others using sonochemical reactions, especially in ethylenediamine.<sup>14</sup> However, this method (sonochemistry) and solvent (ethylenediamine) were found to be unsuitable for the preparation of silver tellurides. An additional disadvantage of ethylenediamine is its high affinity for complexation. This is the reason that the resulting compounds have a relatively high level of carbon impurities and even incorporation of ethylenediamine in the resulting product.<sup>15</sup> Therefore, we developed a different method for the preparation of tellurides and selenides, which is easily implemented using ultrasound irradiation and which is free of the disadvantages of the

\* To whom correspondence should be addressed.

<sup>†</sup> Bar-Ilan University.

<sup>‡</sup> Jerusalem College of Technology.

(1) Xu, R.; Husmann, A.; Rosenbaum, T. F.; Saboungi, M.-L.; Enderby, J. E.; Littlewood, P. B. *Nature* **1997**, *390*, 57–60.  
 (2) Parkin, S. S. P. *Ann. Rev. Mater. Sci.* **1995**, *25*, 88–357.  
 (3) Rao, C. N. R.; Cheetham, A. K. *Chem. Mater.* **1996**, *8*, 2421–2432.  
 (4) Carara, M.; Gundel, A.; Baibich, M. N.; Sommer, R. L. *J. Appl. Phys.* **1998**, *84*, 3792–3797.  
 (5) Jin, S.; Tiefel, T. H.; McCormack, M.; Fastnacht, R. A.; Ramesh, R.; Chen, L. H. *Science* **1994**, *264*, 413–415.  
 (6) Dieny, B. *J. Magn. Magn. Mater.* **1994**, *136*, 335–359.  
 (7) Chan, J. Y.; Kauzlarich, S. M.; Klavins, P.; Shelton, R. N.; Webb, D. *J. Phys. Rev. B* **1998**, *57*, R8103–R8106.  
 (8) Ramirez, A. P.; Cava, R. J.; Krajewski, J. *Nature* **1997**, *386*, 156–159.  
 (9) Gonen, Z. S.; Fournier, P.; Smolyaninova, V.; Greene, R.; Araujo-Moreira, F. M.; Eichhorn, B. *Chem. Mater.* **2000**, *12*, 3331–3336.

(10) Grientschnig, D.; Sitte, W. *J. Phys. Chem. Solids* **1991**, *52*, 805–820.  
 (11) Dalven, R.; Gill, R. *J. Appl. Phys.* **1967**, *38*, 753.  
 (12) Appel, J. *Z. Naturforsch.* **1955**, *10a*, 530.  
 (13) Junod, P. *Helv. Phys. Acta* **1959**, *32*, 567–600.  
 (14) Li, B.; Xie, Y.; Huang, J.; Qian, Y. *Ultrasón. Sonochem.* **1999**, *6*, 217–220.  
 (15) Li, J.; Chen, Z.; Wang, R.-J.; Prospero, D. M. *Coord. Chem. Rev.* **1999**, *190*–192, 707–735.

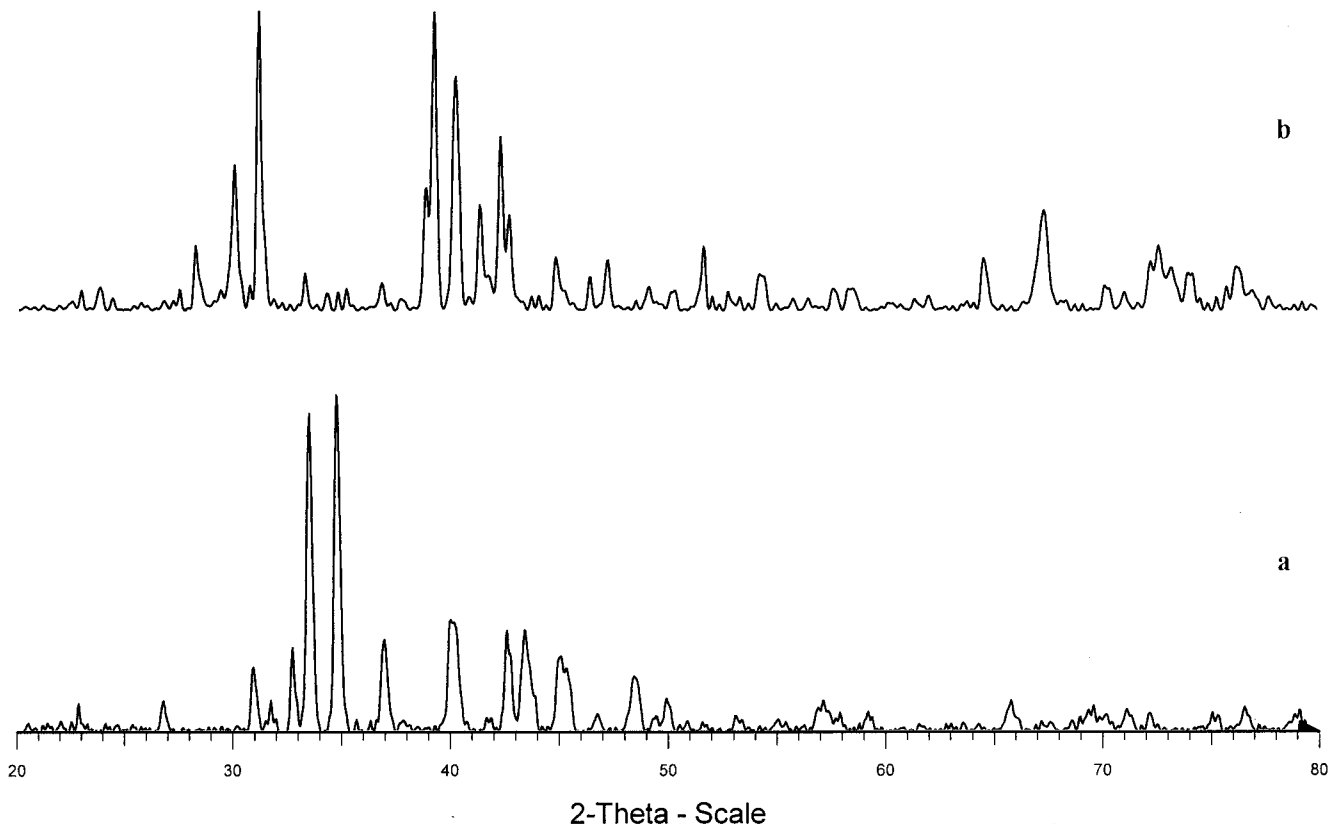


**Figure 1.** Powder XRD patterns of (a)  $\text{Ag}_2\text{Se}$  and (b)  $\text{Ag}_2\text{Te}$ .

ethylenediamine method. To the best of our knowledge, this is the first report of the preparation of  $\text{Ag}_2\text{Se}$  and  $\text{Ag}_2\text{Te}$  using the polyol sonochemical method. Their morphology and properties were studied using various analytical techniques, and these results are reported as follows.

### Experimental Section

All reagents were of the highest commercially available purity. Elemental Te and Se, silver acetate, and ethylene glycol were all purchased from Aldrich Co. and used without further purification. The X-ray diffraction patterns of the products were recorded with a Bruker AXS D8 advance powder X-ray diffractometer (using  $\text{Cu K}\alpha$   $\lambda = 1.5418 \text{ \AA}$  radiation). EDS measurements were carried out using an X-ray microanalyzer (Oxford Scientific) built on a JSM-840 scanning electron microscope (JEOL). High-resolution SEM images were obtained using a LEO Gemini 982 field emission gun SEM (FEG-SEM) operating at 4-kV accelerating voltage. Transmission electron microscopy (TEM) was done on a JEOL-JEM 100SX microscope, working at 100-kV accelerating voltage. High-resolution TEM (HRTEM) images were obtained using a JEOL-3010 set to a 300-kV accelerating voltage. A conventional CCD video camera, with spatial resolution of  $768 \times 512$  pixels, was used to digitize the micrographs, which were then processed using Digital Micrograph software. The EMS package<sup>16</sup> was used to do HRTEM image calculations and electron diffraction indexing. Samples for TEM were prepared by placing a drop of the sample suspension on a copper grid (400 mesh, electron microscopy sciences) coated with carbon film. The sample was then air-dried. Elemental analysis (carbon) was done on an EA 1110 CHNS-O instrument. Differential scanning calorimetric analysis (DSC) was carried out on a Mettler Toledo TC 15, using nitrogen or argon as a purging gas, at a scanning rate of  $5 \text{ }^{\circ}\text{C}/\text{min}$ . The thermogravimetric

analysis (TGA) was done on a Mettler Toledo TGA/SDTA851 instrument using nitrogen or argon as a purging gas, also at a scanning rate of  $5 \text{ }^{\circ}\text{C}/\text{min}$ . Photoacoustic measurements were conducted employing a homemade instrument, which is based on one that was described elsewhere,<sup>17</sup> but with completely updated software. Because of the saturation phenomenon of the photoacoustic signal observed in very black samples, current samples were diluted with  $\text{MgO}$  powder. The ratio of the chalcogenide to  $\text{MgO}$  was 9:1.

Ultrasonic irradiation was provided with a high-intensity ultrasonic probe (Misonix, XL Sonifier, 1.13-cm diameter; Ti horn, 20 kHz,  $60 \text{ W cm}^{-2}$ ) immersed directly into the reaction solution. The reactions were gently cooled with a water bath. All sonochemical reactions were conducted at  $75\text{--}80 \text{ }^{\circ}\text{C}$ . The temperature during the reactions was measured continuously using a digital thermocouple.

**Procedure for Ultrasonic Reaction.** Silver acetate was dissolved in ethylene glycol by gently heating in the sonicator for  $\approx 1$  min. Stoichiometric quantities of Te or Se powder were then added. The system was purged for a few minutes with nitrogen and then the reaction continued for 2 h.

The postreaction treatment procedure included centrifugation, first with the mother liquid and then a few times with  $\text{EtOH}$ , at  $20 \text{ }^{\circ}\text{C}$ , at 9000 rpm. The products were dried overnight under vacuum.

### Results and Discussion

**PXRD Studies.** XRD patterns of the as-prepared  $\text{Ag}_2\text{Se}$  and  $\text{Ag}_2\text{Te}$  are shown in Figure 1a,b. For both products pure phases were obtained. For the  $\text{Ag}_2\text{Se}$  (see Figure 1a), the low-temperature phase,  $\beta\text{-Ag}_2\text{Se}$ , was obtained. The accepted crystal structure of the  $\beta\text{-Ag}_2\text{Se}$  is orthorhombic (its anions form a body-centered cubic

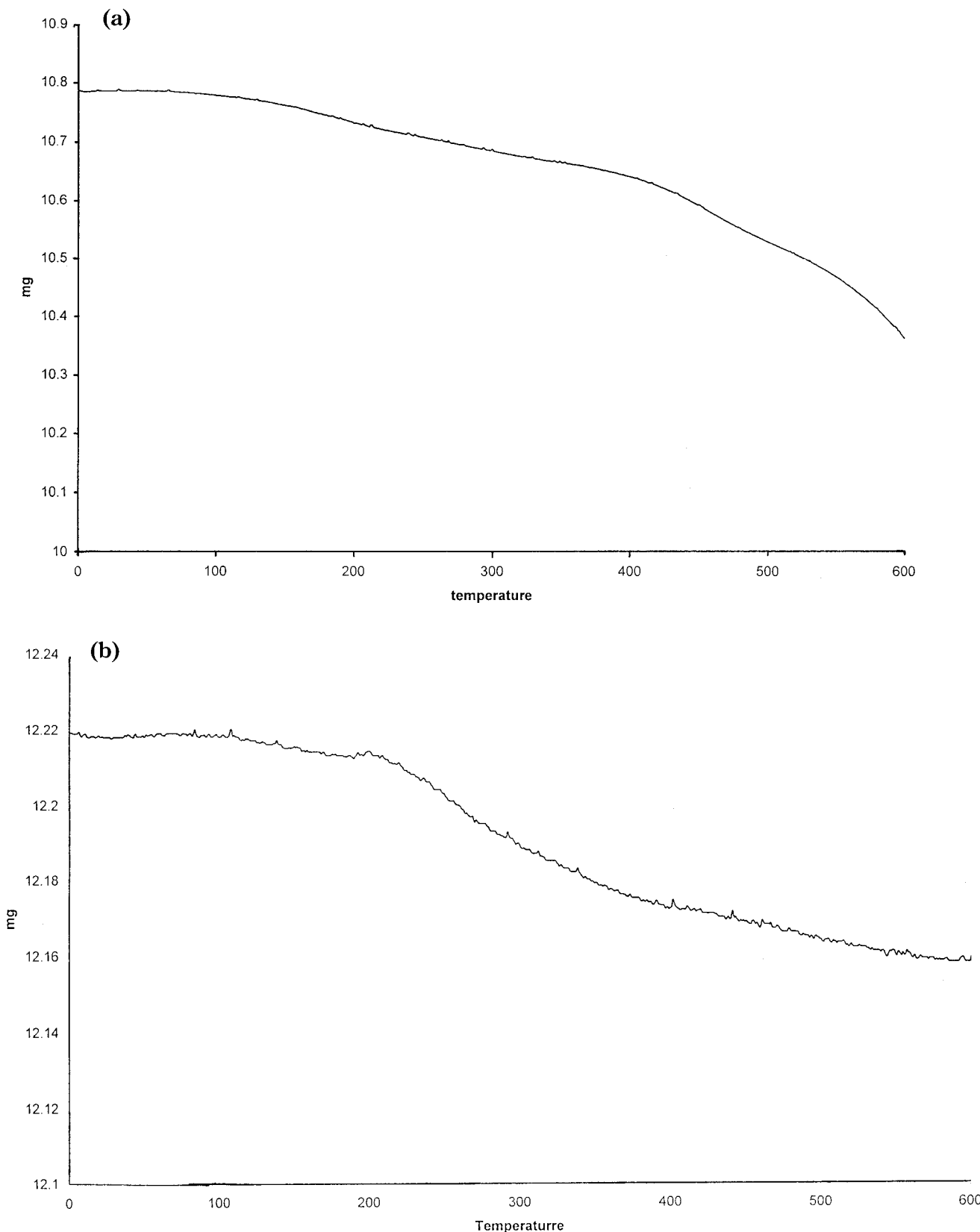


**Figure 2.** TGA measurements (5 °C/min, Ar or  $\text{N}_2$  purging gas): (a)  $\text{Ag}_2\text{Se}$ ; (b)  $\text{Ag}_2\text{Te}$ .

sublattice) with the  $P2_12_12_1^{19}$  space group. The measured lattice parameters are  $a = 0.434$  nm,  $b = 0.706$  nm, and  $c = 0.778$  nm, which agree with the published

data (PDF #24-1041). Observation of the orthorhombic structure for  $\text{Ag}_2\text{Se}$  suggests that this compound is very close to its stoichiometry because for the nonstoichiometric compounds other crystal structures were found. Some broadening of the peaks is observed, and with the Scherrer equation the average particle's dimension was

(18) Krupnikov, E. S.; Aliev, F. Y.; Kerimov, I. G. *Sov. Phys. Solid State* **1979**, 1829–1830.

(19) Ubelohde, A. R. *Q. Rev. Phys.* **1957**, 11, 246.

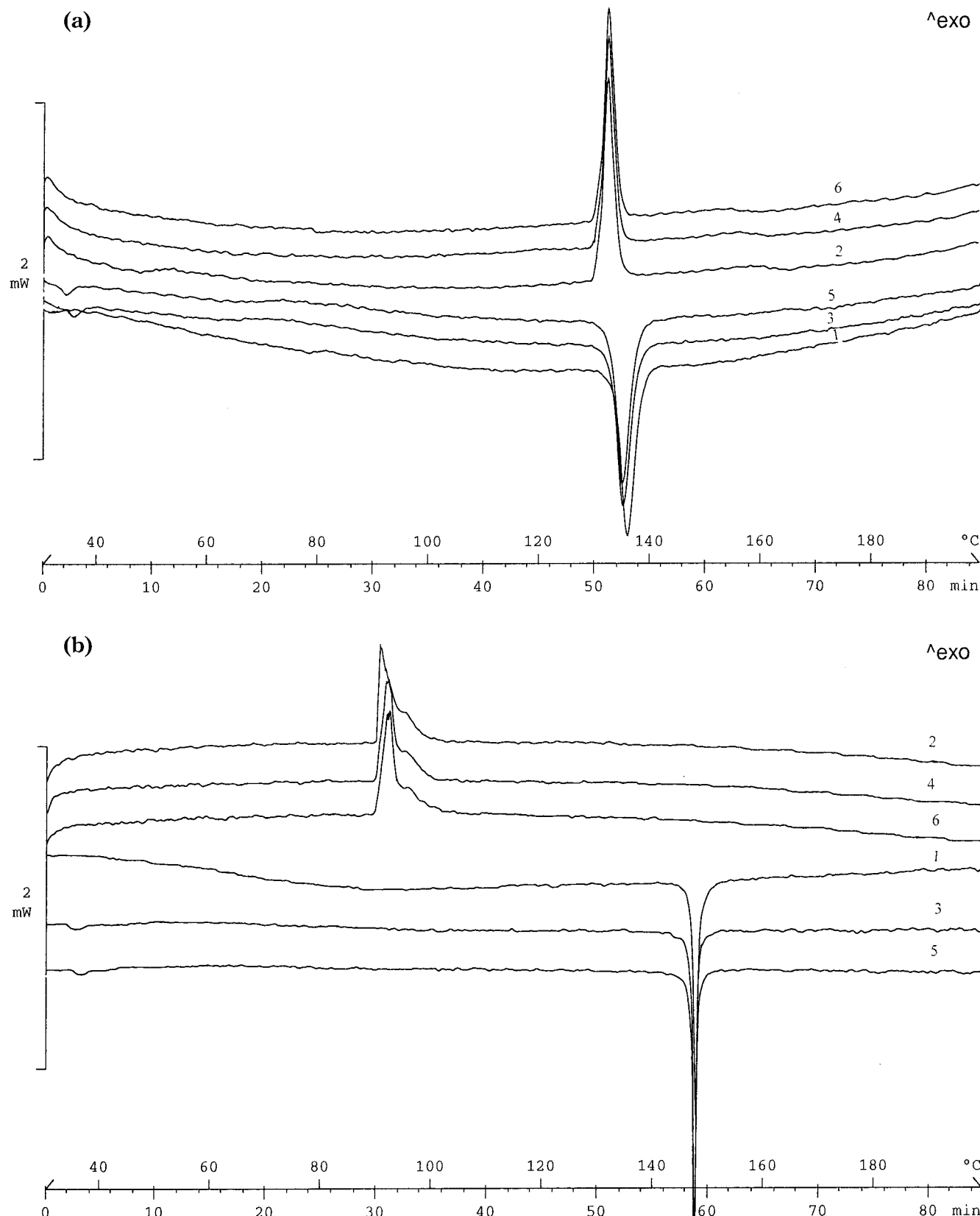


**Figure 3.** DSC curves of (a)  $\text{Ag}_2\text{Se}$  (curves 1, 3, 5: heating; 2, 4, 6: cooling); (b)  $\text{Ag}_2\text{Te}$  (curves 1, 3, 5: heating; 2, 4, 6: cooling).

calculated as 28 nm. For  $\text{Ag}_2\text{Te}$ , the low-temperature  $\alpha$ - $\text{Ag}_2\text{Te}$  phase was obtained. The crystal structure of  $\alpha$ - $\text{Ag}_2\text{Te}$  is monoclinic, space group  $P2/n$ .<sup>13</sup> The calculated lattice parameters are  $a = 0.816$ ,  $b = 0.892$ ,  $c = 0.806$ , and  $\beta = 112.8^\circ$ , which is in agreement with published data (PDF #34-142). Note that the monoclinic

$\alpha$ - $\text{Ag}_2\text{Te}$  phase is a multilayer compound, where the Ag and Ag–Te atomic layers are arranged in the  $\text{Ag}_2\text{Te}$  crystal parallel to the (121) plane (see insert in Figure 1b). Grain dimension calculated using the Scherrer equation was found to be 43 nm. It is known that very small grain size is an undesirable property for magne-

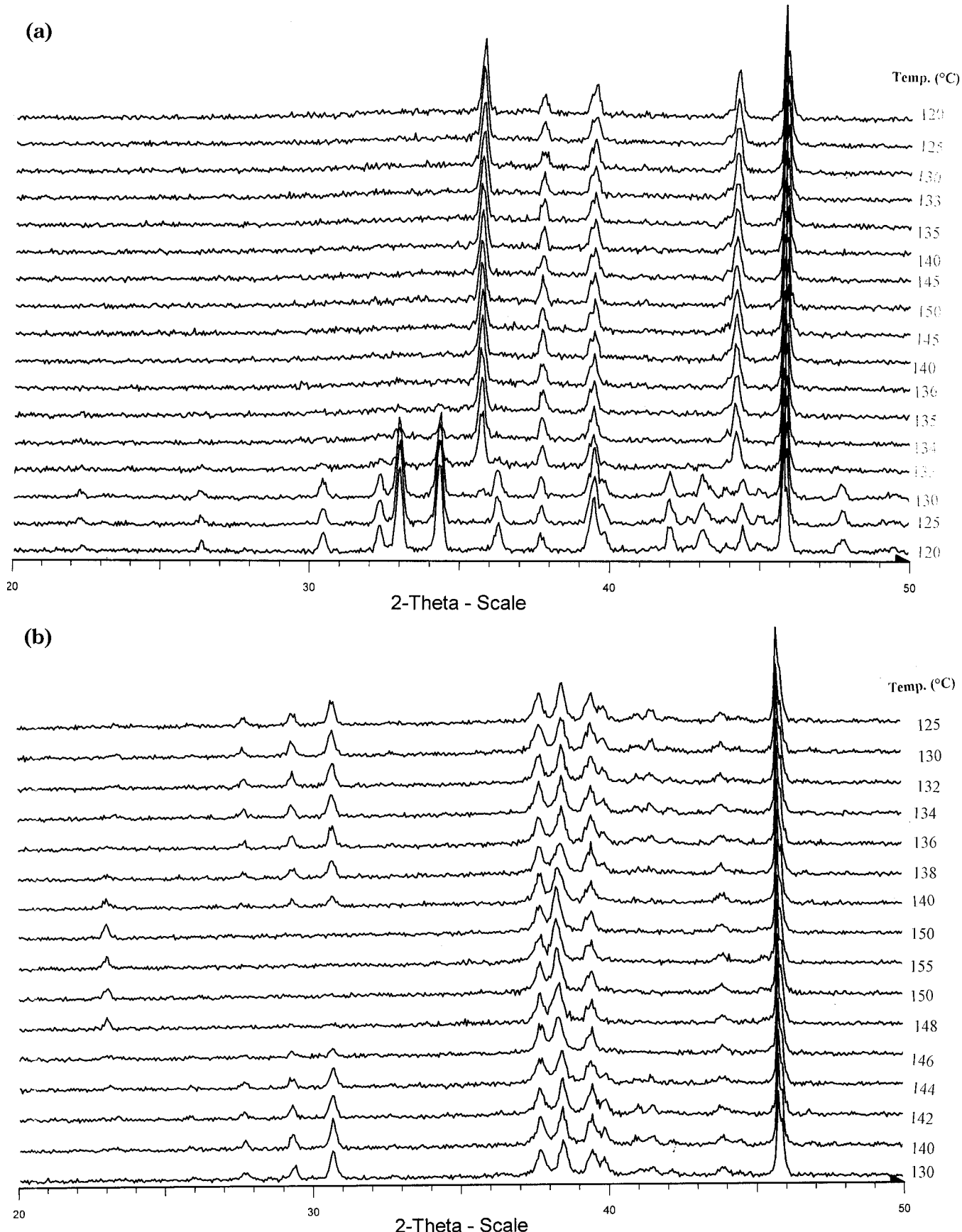


**Figure 4.** Powder TP-XRD patterns of (a)  $\text{Ag}_2\text{Se}$  and (b)  $\text{Ag}_3\text{Se}$ .

toresistance. This is because the MR decreases with decreasing particle dimensions and even disappears when the particle size is less than a few nanometers.<sup>18</sup>

For this reason, all of our reactions were conducted at elevated temperatures, and not with the strong cooling that is usually recommended for sonochemical reactions.

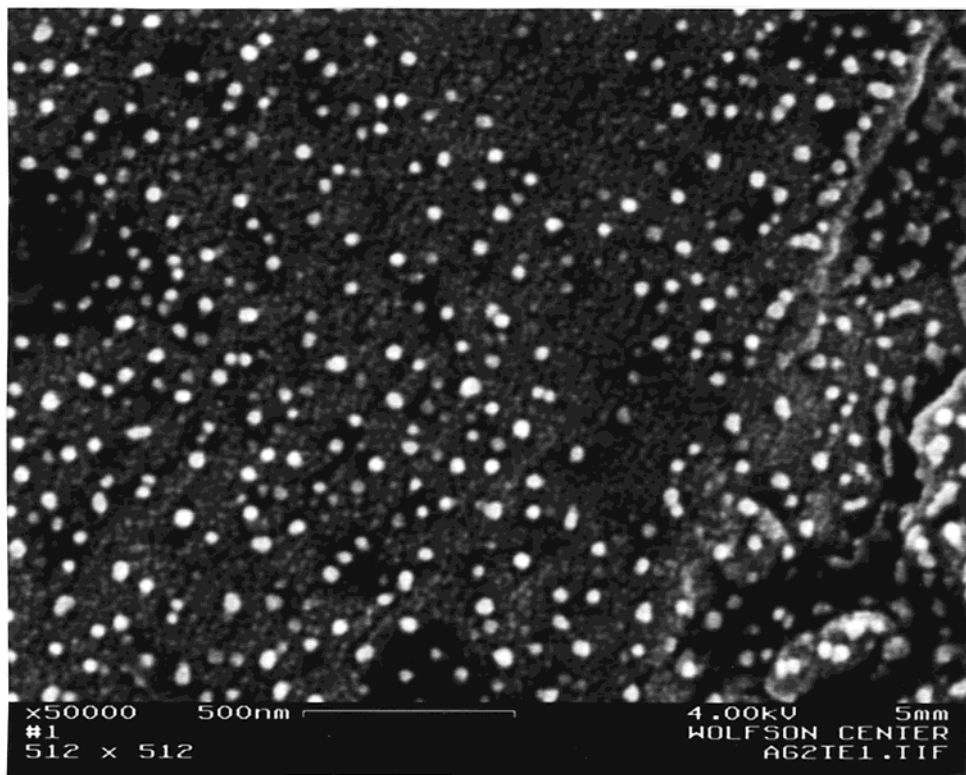


**Figure 5.** HR-SEM image of  $\text{Ag}_2\text{Te}$ .

We believe that the high temperatures resulted in fabrication of larger nanoparticles.

**TGA Measurements.** For both compounds, TGA analysis was conducted to reveal the presence of any chemically adsorbed species (see Figure 2a,b). For both products, almost no mass loss was observed (<0.17%). The TGA-MS measurements reveal that ethylene glycol is not adsorbed on the surface of the particles. The small mass loss that is observed is probably due to desorption of water molecules from the surface of the particles. Elemental analysis conducted on the products showed that the quantity of carbon for both compounds is in the range of 0.1%, which is consistent with the TGA measurements. Results of this analysis are very important for electrical and thermal measurements because the presence of even small amounts of organic impurities on the surface of the nanoparticles can profoundly alter the electric and thermal properties of the material.

**DSC and TP-PXRD Studies.** Polymorphic phase transitions to a superionic conduction phase are observed in many superionic conductors. All silver chalcogenides undergo such reversible first-order phase transitions around 140 °C. To study the phase-transition phenomenon, DSC measurements were done. DSC curves for  $\text{Ag}_2\text{Se}$  and  $\text{Ag}_2\text{Te}$  are shown in Figure 3a,b, respectively. For both compounds, the data show a first-order reversible phase transition. For  $\text{Ag}_2\text{Se}$ , a hysteresis of  $\approx 3.5$  °C in the phase transition was detected. The heating phase transition was observed at 135 °C. A broad hysteresis phenomenon was observed for  $\text{Ag}_2\text{Te}$  (see Figure 3b), where the phase transition (at 148 °C) is also reversible but shows a hysteresis of 56 °C. The hysteresis magnitude was independent of the type of glycol used for its preparation. Three different glycols were used in these experiments. The origin of the hysteresis might be due to different nucleation times

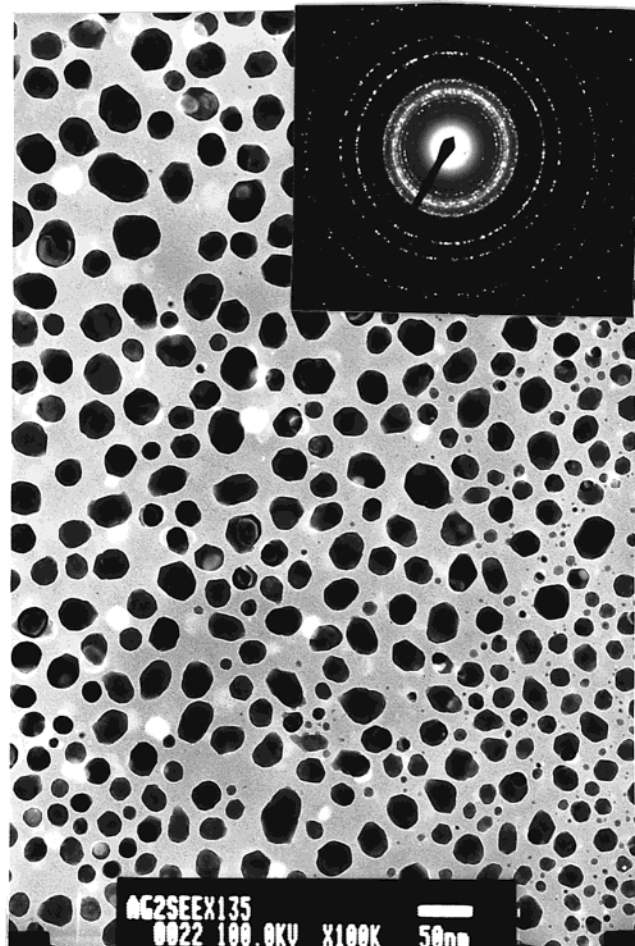


**Figure 6.** TEM pictures of  $\text{Ag}_2\text{Se}$ .

being required for the first step in the phase transition, the nucleation growth,<sup>19</sup> which might result from a

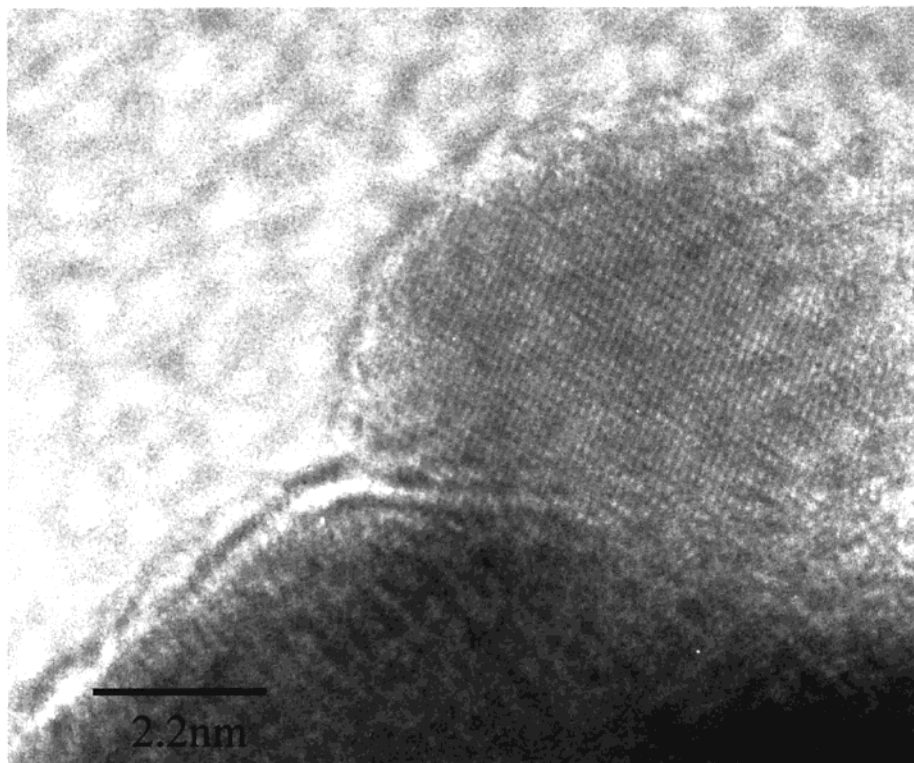


**Figure 7.** HR-TEM image of  $\text{Ag}_2\text{Te}$ .

difference in activation energy for the forward and backward phase transitions. Rao and co-workers demonstrated<sup>20</sup> that an increase in the particles' size reduces the hysteresis temperature. Rao's result does not concur with the differences observed between  $\text{Ag}_2\text{Se}$  and  $\text{Ag}_2\text{Te}$ . We detected a much larger hysteresis for  $\text{Ag}_2\text{Te}$  (16 times bigger), whereas its particles are bigger than those of  $\text{Ag}_2\text{Se}$ . Low-temperature DSC measurements (from room temperature to 133 K) were also conducted, and for both compounds featureless curves were obtained (data not shown).

Results of the variable temperature PXRD measurements for both compounds are shown in Figure 4a,b. For both compounds the phase transition is seen to be reversible. Temperature-programmed PXRD cannot be used for kinetic studies of the phase because this is an isothermal measurement, done under equilibrium conditions. The hysteresis observed in the PXRD data is opposite to that obtained from DSC measurements. For  $\text{Ag}_2\text{Te}$ , the hysteresis is  $\approx 3$  °C and for  $\text{Ag}_2\text{Se}$  it is 29 °C. These results show that the hysteresis temperature may be a function not only of particle size, rate of heating, and the presence of impurities but also of the mass of the studied sample (in the case of PXRD the mass was smaller than in the case of DSC). This also might explain the different temperature values reported in the literature for the phase transitions of these compounds.<sup>21</sup>

The high-temperature phase obtained for  $\text{Ag}_2\text{Se}$  is the cubic phase, space group  $Im\bar{3}m$  ( $\text{Cu}_2\text{O}$ -type structure) with lattice parameters equal to 4.985 Å, in agreement

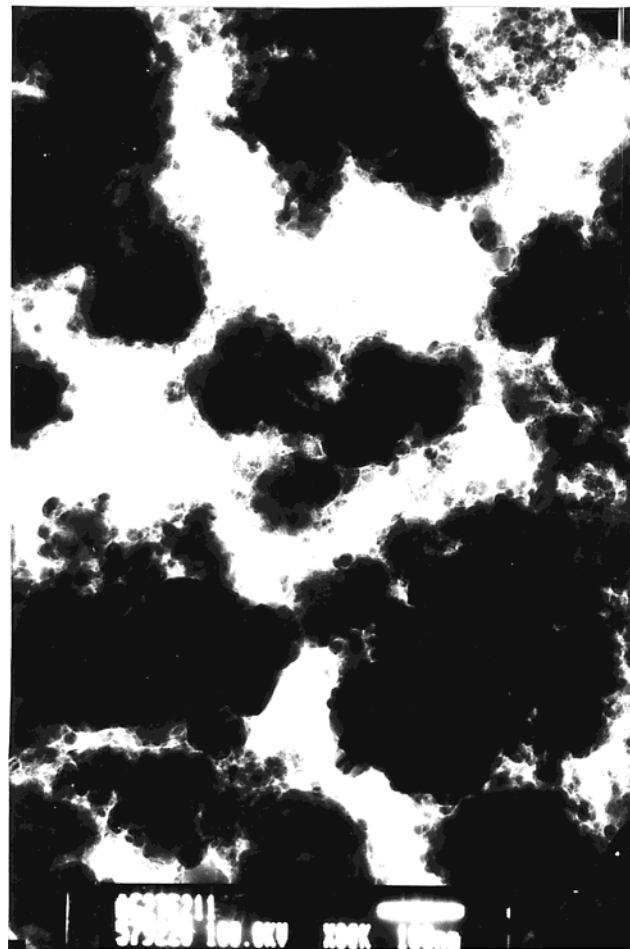


**Figure 8.** TEM image of  $\text{Ag}_2\text{Te}$  sample with 15% excess of Ag.

(20) Natarajan, M.; Das, A. R.; Rao, C. N. R. *Trans. Faraday Soc.* **1969**, *65*, 3081.

(21) Ridder, R.; Amelinckx, S. *Phys. Status Solidi A* **1973**, *18*, 99–107.

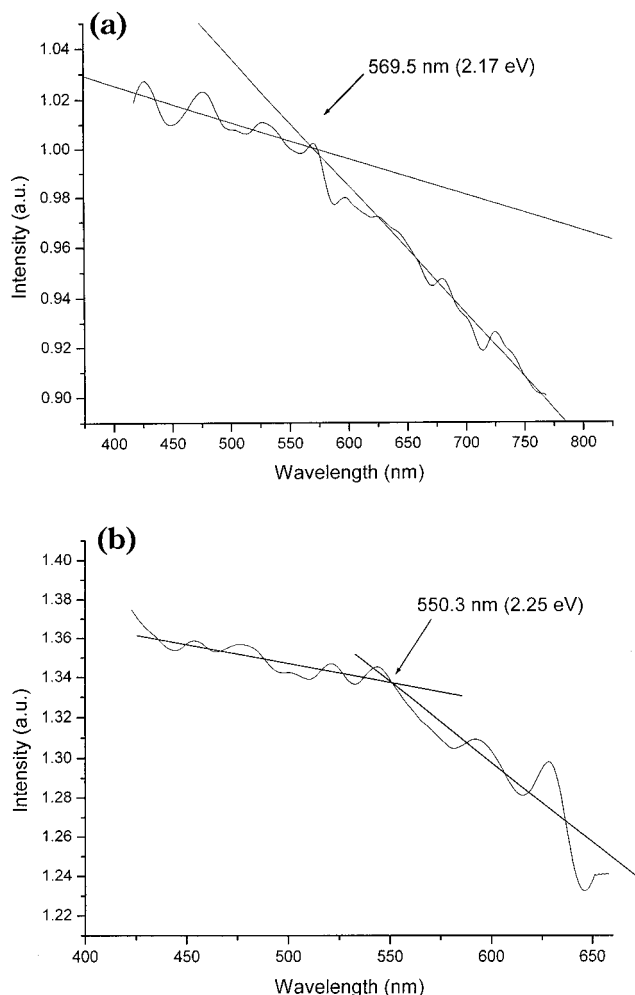


**Figure 9.** PAS measurements of (a)  $\text{Ag}_2\text{Se}$  and (b)  $\text{Ag}_2\text{Te}$ . The positions of band gaps are shown by the arrow.

with published data.<sup>13</sup> The high-temperature phase of the  $\text{Ag}_2\text{Te}$  is also found to be cubic. However, a closer examination reveals that two cubic phases (both in the  $Fm\bar{3}m$  space group) are present, having different lattice parameters that are equal to 6.68 and 6.58 Å.

**Electron Microscopy Studies (TEM, HR-SEM, and HR-TEM).** One of the problems faced in working with silver chalcogenides in TEM measurements is the very high sensitivity of both compounds toward the electron beam.<sup>22</sup> Polymorphic transitions are known to be induced by the electron beam, resulting in specimen movement. This phenomenon has been observed by others.<sup>21</sup> Both chalcogenides have spherical morphology, as shown, for example, for  $\text{Ag}_2\text{Te}$  in Figure 5 (HR-SEM image). The sample is seen to consist of spherical particles, monodispersed, with an average diameter of 47 nm. This result is in agreement with XRD data (Scherrer calculation yields 43 nm as the average size). The agreement of the XRD and the HRTEM data leads us to conclude that these spheres are single crystals of  $\text{Ag}_2\text{Te}$ .

Nanocrystals of  $\text{Ag}_2\text{Se}$  are smaller than those for  $\text{Ag}_2\text{Te}$ ; their average diameter is 31 nm, and they are also not aggregated (see Figure 6). The  $\text{Ag}_2\text{Se}$  spheres also

appear to be single crystals, as shown by the close agreement with the XRD grain size measurement (28 nm).

HR-TEM measurements are also done to study the aggregation mode and the surface properties of  $\text{Ag}_2\text{Te}$ . A representative HR-TEM micrograph is shown in Figure 7. We observe that very small particles are attached to the surface of the big particles. Analysis of the atomic interplanar distances revealed that these are silver nanoparticles, with an average diameter of 7–8 nm. For every large particle of  $\text{Ag}_2\text{Te}$ , about 2–3 small silver clusters are observed. Separated and isolated Ag nanoparticles were not detected in our measurements.

Previous measurements in bulk samples showed that some stoichiometric excess of silver in the silver chalcogenides, especially in  $\text{Ag}_2\text{Te}$ , improves the MR (magnetoresistance) properties tremendously.<sup>1</sup> This was the reason that in all our experiments the mixture of the reactants was always richer in the silver containing precursor. The HR-TEM data show that the excess silver forms clusters on the surface of the  $\text{Ag}_2\text{Te}$  particles. For an excess of 1% silver, we find 3–4 nanoclusters of the silver on the surface of every  $\text{Ag}_2\text{Te}$  particle (for example, see Figure 7). To confirm affinity of the silver clusters to the  $\text{Ag}_2\text{Te}$ , we synthesized  $\text{Ag}_2\text{Te}$  using a 15% excess of silver salt. The HRTEM images of this material show that silver clusters are almost exclusively attached to the surface of the bigger particles of silver telluride (Figure 8).

The electronic properties of the products were studied by measurement of the optical absorption spectra using photoacoustic spectroscopy (see Figure 9 a–b). The “knee” method was used to estimate the band gap.<sup>23</sup> For  $\text{Ag}_2\text{Se}$  and  $\text{Ag}_2\text{Te}$ , band gaps were found at 569.5 nm (2.17 eV) and 550.3 nm (2.25 eV), respectively. This is especially interesting because both compounds are known to be narrow-band semiconductors, with published band gap values of 0.15 eV for  $\text{Ag}_2\text{Se}$ <sup>24</sup> and 0.67 eV for  $\text{Ag}_2\text{Te}$ .<sup>25</sup> The difference between published values and PAS measurements cannot be explained by blue shift due to the fact that the difference is relatively high and the nanoparticles were more than 10 nm in diameter. On the basis of the slope of the band gap, we could presume that for both compounds we have indirect band gaps. As far as we know, this is first time that band gaps at  $\approx 2.2$  eV for this compounds were observed. One of the reasons for this may be the high sensitivity of PAS relative to other classical methods such as diffuse reflectance.

**Mechanism of the Formation of the Nanoparticles.** The sonochemical reactions leading to the formation of silver chalcogenides are another example of the polyol-assisted preparation of the chalcogenides. We found that two conditions are necessary for the reaction to proceed: (a) the metal ion must be reduced by the polyol solvent; (b) the reaction must have a very high thermal activation. Condition (a) is fulfilled for the silver. It is known that silver salts are easily reducible

(23) Rosencwaig, A. *Photoacoustics and Photoacoustic Spectroscopy*; Academic Press: New York, 1980.

(24) Junod, P.; Hediger, H.; Kilch, B.; Wullshleger, J. *Philos. Mag.* **1977**, *36*, 941.

(25) Appel, J. *Z. Naturforsch.* **1995**, *10A*, 530.

by any polyol solvent, for example, ethylene glycol, by regular heating for a few hours.<sup>26</sup> Condition (b) is satisfied by using sonication. During sonochemical reactions, very high temperatures, up to a few thousand degrees Celsius, can be achieved. These high temperatures provide the activation energy required to drive the reaction to completion. We have demonstrated that for many ions the polyol-assisted reaction can be effected using microwave irradiation to heat the reaction mixture. However, we have been unable to obtain silver chalcogenides by employing microwave heating. Instead, we obtained pure Ag (PDF # 04-0783) as the main product, together with a very small amount of silver chalcogenide (<5%). After only a few minutes of the microwave-heated reaction, the precipitation of the metallic silver was observed. The heating of the metallic particles by the microwave radiation was apparently not enough to cross the activation barrier of the chalcogenide oxidation. As a result, the silver particle grows, becomes too large, and precipitates before the reaction of chalcogen with silver could proceed (>25 nm). These solid state reactions are diffusion-limited so that the presence of large particles of silver prevents full interdiffusion of the silver into the chalcogen. This is the reason that, even after prolonged microwave irradiation, only small quantities of the Ag<sub>2</sub>Te or Ag<sub>2</sub>Se are obtained.

(26) Fievet, F.; Lagier, J. P.; Figlarz, M. *MRS Bull.* **1989**, Dec, 29–34.

In this case, the sonochemical reaction is superior to the microwave because it provides a mechanochemical effect that is exclusive to sonochemical reactions. Ultrasound can break big crystallites into smaller ones, and such small nanoparticles have a higher reactivity toward the formation of the binary chalcogenides. As a control reaction, regular heating (reflux) of the same mixture of precursors was carried out for 48 h (under Ar), and the formation of silver chalcogenides was not observed. Instead, 100-nm particles, which contain mostly silver (PDF # 04-0783), a small amount of Te, and some Ag<sub>2</sub>Te (<10%) are obtained. None of these control reactions lead to the formation of stable colloids. Instead, the chalcogen precipitated very easily. This is not the behavior observed in a microwave or a sonochemical reaction, where the product does not precipitate easily.

### Conclusions

In this work, we demonstrate that the polyol reaction can be used sonochemically, but not with microwave radiation, to synthesize silver telluride and selenide. Both products were prepared with nanometer dimensions and were characterized using different physical analytical methods such as XRD, electron microscopy, and thermal analysis. In a second paper, the results of the electrical, thermoelectrical, and magnitoresistance measurements will be reported.

CM010810P